# Adsorption of Block Copolymers from Selective Solvents on Curved Surfaces

**Eli Hershkovits,[†] Allen Tannenbaum,[†,‡,||] and Rina Tannenbaum*[,§,⊥]**

*School of Biomedical Engineering, School of Electrical and Computer Engineering, and School of Materials Science and Engineering, Georgia Institute of Technology, Atlanta, Georgia 30332, and Department of Electrical Engineering, Department of Chemical Engineering, Technion—Israel Institute of Technology, Haifa, Israel*

*Received December 5, 2007; Revised Manuscript Received February 19, 2008*

ABSTRACT: We have investigated the adsorption of asymmetric poly(styrene-*b*-methyl methacrylate) block copolymers (PS−PMMA) from a selective solvent onto alumina ($Al_2O_3$) particles having variable and controllable radii. The solvent used was a bad solvent for the PS block (block A) and a good solvent for the PMMA block (block B), which has a higher affinity of the surface. Such a case represents a new class of adsorption, where both blocks compete for the adsorption sites of the metallic surface. Two theoretical models, the modified drops model and the perforated film model, have been evaluated as appropriate representation of such an adsorption scenario. The experimental results indicated that the adsorption of the PS−PMMA block copolymer generated a patterned surface comprised of a homogeneous melt layer of the PS block perforated with holes having a variable PMMA structure, depending on the distance from the bottom of the hole (alumina surface) and the distance from walls of the hole. The density gradient of the PMMA moiety in the hole reverted to the classical brush morphology at a critical distance from the surface of the hole.

## 1. Introduction

The adsorption of polymer chains onto metallic or metal oxide substrates is governed by a competition between the interfacial contact energy of the polymer segments with the substrate,[1–3] the entropic energy penalty due to the conformational changes of the surface-confined polymer chains,[4,5] and the interactions between the polymer and the solvent.[6–11] Moreover, the polymer adsorption is facilitated by an interaction-multiplier effect, which is unique to chain molecules.[12–14] Any interaction that occurs with one segment is multiplied by the large number of identical segments in the macromolecule to generate a large intermolecular effect. Therefore, polymers tend to bind irreversibly to metallic surfaces, even via the mechanism of relatively weak segment-level interactions. As a consequence, such reactive segments can form permanent bonds with the metallic surface, resulting in a dense packing of the polymer chains, thus significantly reducing the number of available reactive sites on the metallic surface.

This behavior has been responsible for the extensive use of polymer as stabilizing agents in the synthesis of metallic nanoparticles.[15–18] The adsorbed polymer chains act as steric and hydrophobic barriers that prevent the aggregation of the metallic clusters beyond an equilibrium size, thus imparting a stabilizing effect on the nanoparticles. Hence, polymer adsorption plays a major role in the control of particle size during polymer-mediated particle synthesis and on the characteristics of the particle suspensions in the polymer solutions.[18–25] Moreover, the adsorption of polymers on metallic substrates can also serve to modify and pattern the chemical properties of the surfaces according to the chemical nature of the polymer, the extent and nature of the metallic particle/polymer interfacial interactions, and the resulting surface morphology of the adsorbed layer. In order to provide additional degrees of freedom that would enable the control of structural properties of the adsorbed layer, recent work utilized systems that include block copolymers having blocks with dissimilar chemical features.[26–28] In these systems, polymer adsorption will be governed by the specific interfacial interactions of each block with each other, with the surface, and with the solvent.

In previous studies it has been shown, both theoretically and experimentally,[29–32] that the characteristics of the adsorbed polymer layer are strongly dependent on the radii of the substrate particles. In order to highlight the specific role that the size of the adsorbing particle imparts on the extent of polymer adsorption, we limited ourselves to one type of polymer and followed its adsorption on surfaces that differed only in the magnitude of their curvature, i.e., from flat surfaces to very small particles, but consisted of the same chemical makeup. Our fundamental premise was that the details of the segment-level chemistry were independent of surface curvature since the Kuhn length of the monomers was at least 1 order of magnitude smaller than the size of the smallest particles probed,[33,34] and hence, the variations of the amount of polymer adsorbed and the density of contact points between the polymer and the surface of the particles were exclusively a result of the variations in particle sizes.

A similar approach was used also in order to probe the adsorption characteristics of block copolymers on surfaces with varying degrees of curvature. The experimental setup consisted of suspensions of $Al_2O_3$ particles in solution of block copolymers, poly(methyl methacrylate-*b*-styrene), i.e., PMMA−PS diblocks, and solvents with different degrees of selectivity to either blocks. As previously shown, there was a preferential affinity of the PMMA block to the $Al_2O_3$ surface as compared to that of the PS block.[24,25,32] Under these conditions, the properties of the solvent, and specifically the interactions between the individual blocks and the solvent, will constitute the crucial driving force that would govern the adsorption of the block copolymer on the surface.[25]

* Corresponding author. E-mail: rinatan@mse.gatech.edu.
[†] School of Biomedical Engineering, Georgia Institute of Technology.
[‡] School of Electrical and Computer Engineering, Georgia Institute of Technology.
[§] School of Materials Science and Engineering, Georgia Institute of Technology.
[||] Department of Electrical Engineering, Technion—Israel Institute of Technology.
[⊥] Department of Chemical Engineering, Technion—Israel Institute of Technology.

10.1021/ma702706p CCC: $40.75 
Published on Web 04/12/2008

Theoretical mean field and scaling methods have been employed to analyze adsorption of block copolymers from nonselective solvents for flat as well as for spherical surfaces.[35–40] These studies suggested the formation of a bilayer structure comprised of a self-similar anchor layer, i.e., the PMMA block, and a brush, comprised of the unadsorbed block, i.e., the PS block. The dimensions and concentrations of these layers are controlled to a large extent by the relative size of the blocks.[41–43] Our results showed good correlation between the theory and the experimental data for the case when the adsorbed polymers are dense enough, i.e., when the solvent is a good solvent for PS block and a Θ-solvent for the PMMA block. However, in the case when the adsorption layer is dilute, i.e., when the solvent is a good solvent for both blocks, the PMMA adsorption layer at the surface becomes less dense, and the grafted PS moiety exhibits a transitional morphology between a brush-like and a bubblewrap-like ("quasi-brush") layer.

These observations have important implications regarding the surface properties of polymer-coated metal and metal oxide substrates. In particular, the stratification of the adsorbed polymer layer in the case of the adsorption of diblock copolymers on curved substrates may impart specific functionality and chemical reactivity to such particles. These properties may prove crucial in a variety of applications where the use of such surface-tailored particles is being considered.

Adsorption of block copolymers from a selective solvent, i.e., a solvent that is good for one block but bad for the other, has been shown experimentally[44–50] to create, under certain conditions, only partial coverage of the surface. This phenomenon is characterized by the appearance of surface micelles with a core made of a melt of the solvophobic core and a corona that consists of the solvated blocks. The micelles can undergo a phase transition to a lamellar phase, as well as other phases, upon their adsorption. This fact indicates that with proper control a micropatterning of the surface is possible.

Joanny has used a mean-field approach to analyze the case of a diblock copolymer (A−B blocks) in a preferential solvent,[39,40] for the case where both blocks do not reactively interact with the flat surface. In addition, both blocks were assumed to be strongly incompatible. Following these assumptions, it was found that the adsorption created a uniform bilayer, where the first layer, which was in a direct contact with the surface, was made of a melt of the monomers of block A and the second one is a brush of the block B. The exact thickness of these layers depended on the bulk density of the polymers. The model predicted a transition of the uniform adsorption layer into a lamellar structure only when the block copolymers were in the lamellar phase in the bulk. Ligoure suggested a solution to a case where the A block only partially wetted the flat surface. In this case,[51] the solvophobic blocks form droplets of melt on the surface with a brush corona made of the B blocks, as shown in Figure 1. It was shown that the shape of the drop is perturbed only slightly from the classical shape that is dictated by the Young model that predicts that the drop edge will form an angle $\vartheta_0$, i.e., the Young angle, which measures the spreading power of the monomers of A on the surface. This case was explored numerically with a Monte Carlo method.[51] Adsorption under similar conditions but with strong interactions of the monomers of block A with the surface have been treated by mean-field methods,[46] and surface micellization was found also in this case.

In the current work we have investigated the adsorption of asymmetric PS−PMMA block copolymers (i.e., with various compositions) from a selective solvent on alumina ($Al_2O_3$) particles having variable and controllable radii. The solvent used was a bad solvent for the PS block (block A) and a good solvent for the PMMA block (block B). As previously shown, the PMMA monomers interacted weakly (by the deGenne definition[52]) with the surface of the alumina substrates. Such a case represents a new class of adsorption, where both blocks compete for the adsorption sites of the metallic surface.

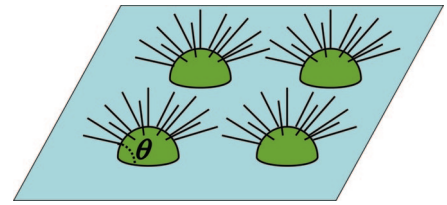


**Figure 1.** Schematic representation of the drops model in which the adsorbing polymer blocks partially wet the surface. The solvophobic blocks (monomers A) assume a drop-shaped core and have an associated brush-like corona formed by the solvophilic blocks (monomers B). The kernel has a contact angle that is slightly perturbed from the classical Young angle: $\cos \vartheta_0 = (\gamma_{ws} - \gamma_{wA})/\gamma_{sA}$, where $\vartheta_0$ is the Young angle that measures the spreading power of monomers A on the surface. The interfacial tension parameters $\gamma_{ws}$, $\gamma_{wA}$, and $\gamma_{sA}$ denote the wall−solvent, wall−A, and A−solvent interfacial tensions, respectively. In this model the drops are assumed to be far apart as to avoid shape deformation due to interdrop interactions.

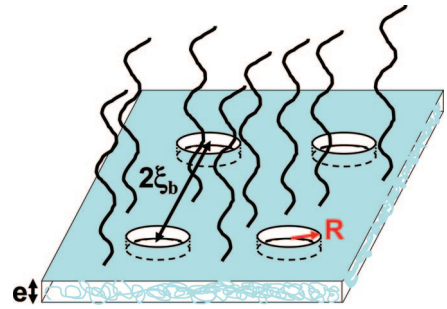


**Figure 2.** Schematic representation of the perforated film model. The spreading power of block "B" is positive, so that block B form a film of melt with a width *e*. Polymer "A" that is desolved in the liquid form a brush with a height "$l_0$". The energy of the brush is high enough to counteract the spreading power of the film. This effect causes the formation of holes in the film. The brush that is grafted to this perforated film has lower density and hence also a lower energy than the brush that is grafted to an intact film.

## 2. The Adsorption Model

In all the models described previously, adsorption from a solution above the critical micelles concentration (cmc) is assumed to form contiguous regions of the adsorbed blocks. Since our solutions were prepared above the cmc, we have employed the same assumption also for our case. Within the boundaries of the contiguous regions, the structure is assumed to be constant. In the region of the adsorbed A monomer, the structure is that of a melt, and in the regions where the B monomers are adsorbed, the structure is the same as the self-similar structure that was described for the homopolymer adsorption case.[36–38]

Assuming the validity of the assumptions regarding the presence of the contiguous regions of the adsorbed block, there are two alternative pictures that can model the adsorption of the PS−PMMA block copolymer in our experiment. The first picture, the "drops model", shown in Figure 1, represents a case where aggregates of the solvophobic blocks form surface micelles (drops). The solvophilic blocks (both from the surface micelles and from the solution) form a uniform adsorption structure in between the drops. The second scenario represents the opposite case, that of a "perforated film", shown in Figure 2, where the solvophobic blocks form a flat film on the surface, having holes that contain a semidilute solution of the adsorbed solvophilic blocks. On the basis of the limits of validity for the

two models, we will advocate in the next section that the second model better corresponds to the correct representation for our results.

**2.1. The Modified Drops Model.** In this work, we will consider a drops model for surface micellization that was developed by Ligoure.[51] Here we will give a short summary of the model. The free energy of the surface micelle is taken to be the sum of three noninteracting terms: a term for the energy of the molten core of the solvophobic monomers, a term that accounts for the energy of the corona made of the semi dilute solution of the solvophilic blocks, and a line energy of the drop contact line.

Ligoure used scaling and geometrical arguments to give a mathematical formulation for these terms. Minimizing the energy expression gives the optimal aggregation size and the optimal contact angle of the formed drops. The value of the contact angle was found to be only slightly perturbed as compared to the classical Young angle given by $\cos \vartheta_0 = (\gamma_{ws} - \gamma_{wA})/\gamma_{sA}$.[51] In this expression, $\vartheta_0$ is the Young angle that measures the spreading power of the monomers A on the surface; $\gamma_{ws}$, $\gamma_{wA}$, and $\gamma_{sA}$ are the interfacial tension parameters of the wall−solvent, wall−A monomers, and solvent−A, respectively. For a small contact angle, which seems to be the case in our experiment, the energy of the corona will increase the wetting.

The degree of micellization of the surface micelles is given by $Q^*(\theta) = f(\theta)Q^*$, where $f(\theta)$ is a smooth increasing function of the contact angle from zero to a constant with a value close to four. The solution micelle aggregation number $Q^*$ is of the order $N_B^{3/11}N_A^{10/11}$, where $N_A$ and $N_B$ are the degrees of polymerization of the two blocks. In order to apply this model to our case, we need to change only the term for the free corona. The partial adsorption of some of the corona B blocks will absorb some of the energy of the corona. The resulting decrease in the corona energy will reduce the total energy from a classical energy of a drop on a wall. Hence, the contact angle is expected to be closer to the classical Young angle than for the case when the B blocks do not adsorb to the surface. This indicates that in case of a competitive adsorption the solvophilic blocks will act to stabilize an array of drops with a classical shape.

This model is valid only when the spreading power $S = \gamma_{ws} - \gamma_{As} - \gamma_{wA}$ is negative and, moreover, when the Young angle is considerably larger than zero. A second limitation for the correctness of the model is that the surface micelles should not interact, which means that they should be far apart from each other. As will be demonstrated in the Results section, both these limits are considerably breached in our experiment.

**2.2. The Perforated Film Model.** When the spreading power $S$ of the solvopobic melt is positive, the adsorbed layer is predicted to have a double-layer structure. The first layer, i.e., the one that is in direct contact with the surface, is made of a thin film of the melt of blocks A. The second layer is a made of a solution of the grafted blocks B. If the density of the grafting points is low, then the B blocks will form isolated mushrooms in the solvent. If it is higher than the brush transition,[53] then the grafted layer is predicted to have a stretched "brush" structure. This model, which was established both experimentally and numerically, was developed specifically for the case when the monomers of the block B are repelled by the surface.

For the case when block B can adsorb onto the surface, the above double-layer structure can become unstable according to the following scenario: The increase of the brush density will increase the confinement energy of the grafted layer. The formation of holes in the film decreases the average brush density and hence causes a decrease of the brush energy. The formation of holes will add energy to the adsorbed system, but beyond a certain critical brush density, the net contribution of the holes to the free energy of the polymers will be negative. Hence, the structure of a perforated film will turn out to be the global minimum of the free energy which will cause it to constitute the equilibrium structure of the adsorption layer.

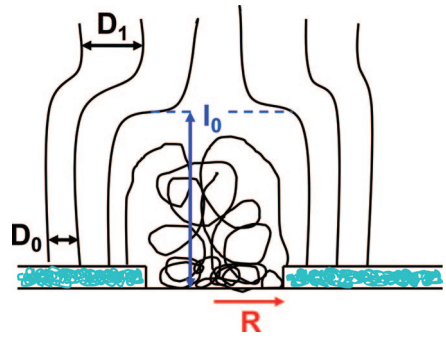


**Figure 3.** Composition of the perforated film model. A hole with a radius $R$ in the film of the A melt modifies the grafted brush structure in two ways: (a) The hole itself is filled with a semidilute solution of blocks B. These blocks interact with the bare surface to form a self-similar adsorption structure as defined by deGennes. It is important to note that this structure does not depend on boundary effects, and hence, it is independent of the concentration outside of the holes region. The self-similar structure occupies a cylinder with a radius $R$ and height $l_0$. Outside of the cylinder the structure of the adsorption layer is the conventional grafted brush structure. At a distance larger than $l_0$ from the surface, the grafted layer forms a uniform brush with a spacing $D_1$ that is larger than the $D_0$ spacing at next to the surface. The resulting decrease in the brush energy is the reason for the stabilization of the structure.

In the following section we will develop a simplified model for the perforated film adsorption, following the schematic description in Figure 2. The model is used to produce an analytical expression for the free energy of the adsorption layer. Employment of energy minimization techniques for this expression generates the composition of the film.

The model assumptions are as follows:

(1) The concentration of the polymers in the solution is high enough to get surface aggregates.[39,40,51]

(2) The spreading power of the A monomers on the surface is positive.

(3) There are two separate phases on the surface: a film of a melt of blocks A with a brush of tails of blocks B and holes with a semidilute solution of the B blocks. The structure inside each phase is homogeneous; i.e., there is no transition region.

(4) Blocks on the edge of the film bend to form a self-similar adsorption structure as described in the deGennes model.[36–38,52] The adsorption layer in the hole has a fixed structure that is independent of its environment. The hole is larger than a typical correlation length of the self-similar structure in the bottom of the adsorption layer. As was noted by deGennes,[36–38,52] this length can be much smaller than the Flory radius of blocks A. We assume that the hole has a perfect cylindrical shape (see Figure 2).

(5) The hairs in the brush are much longer than the height of the self-similar adsorbed volume that is locked in the volume above the holes and is bound by the brush of free hairs, as defined by $l_0$ and shown in Figure 3. For a vertical distance that is larger than $l_0$, the typical distance between the hairs of the brush is $D_1$. This distance defines a hair density $\sigma_1$, and it is larger than the distance between the hairs at the base of this layer, $D_0$, which defines the base hair density $\sigma_0$. The hair density $\sigma_1$ is proportional to the partial coverage of the surface by the film defined by $1 - \Omega$, where $\Omega$ is the partial area occupied by the holes. The energy of the brush is dominated by the contribution of the upper part where the density is uniform. The thickness of the melt $e$ is assumed to be constant.

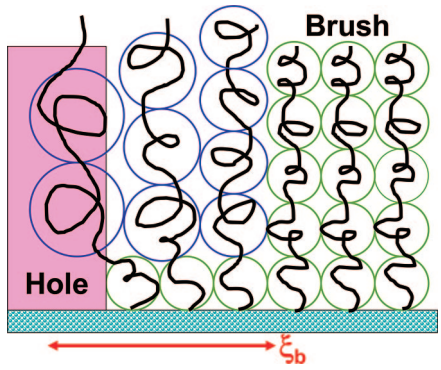


**Figure 4.** Schematic representation of the hole correlation length $\xi_b$. Next to the hole there is spreading of the brush. This spreading is manifested in the blob model by an increase of the radius of the blobs. There is a finite correlation length along which the perturbation that is presented by the hole will influence the brush structure. The enlarged blobs are colored blue and the nonperturbed blocks are green.

(6) For a wide range of block molecular weights, the distribution of the holes is independent of the holes size. We base this assumption on the following two observations: (a) the results[54] from a dewetting experiment on a diblock film indicate that the holes that are nucleated form a distribution that depends only on the thickness of the film and not on the size of the holes; (b) in order to gain the maximal reduction in the energy of the brush, the distribution of the distances between the neighboring hairs on the top layer needs to be constant. We anticipate some screening length $\xi_b$, beyond which the perturbation to the distance between the blocks as presented by the hole will decay to zero. This screening length is much larger than the size of the blobs in the brush (Figure 4). Indeed, theoretical and numerical works suggest the existence of such a parameter with a typical size of $\xi_b = \sigma_0^{-1/6} N_B^{2/5}$ that is by far larger than $\sigma_0^{-1/2}$, which is proportional to the blob radius.[47] For simplicity, we will assume here that $\xi_b$ is a constant that is independent of the radius of the holes. If we assume also that the holes are not much larger than $\xi_b$, we can expect a homogeneous distribution of the holes with typical center-to-center distance of the order of at least $2\xi_b$.

With this set of assumptions, we can write down the following expression for the free energy per unit area of the adsorbed layer:

$$F = (1-\Omega)F_A + \Omega(F_B + F_A^{hole} + F_S) \quad (1)$$

In this expression, the fractional surface coverages $\Omega$ and $1-\Omega$ represent the fraction of the area occupied by regions B and A, respectively. Further, $F_A$ is the free energy per unit area in the film region made of block A, $F_B$ is the free energy of the self-similar adsorption structure in the region made of block B, and $F_A^{hole}$ is the energy that is needed to create a cylindrical hole in a film of the melt having the composition of A. Finally, $F_S$ is the extra energy that is infused into the system by the interaction of block A with solvent on the walls of the holes.

The pure film free energy $F_A$ was determined[39,40] to be

$$F_A = -S - \gamma_{sA}\left(\frac{e}{N_A a}\right) + \left(\frac{H}{12\pi e^2}\right) + \left(\frac{T}{a^2}\right) N_B \sigma_1^{11/6} \quad (2)$$

where $\gamma_{sA}$is the interfacial tension between monomers A and the solvent, $a$ is the monomer size, $H$ is the Hammaker constant, and $T$ is the temperature. Using the assumptions summarized previously (in item 5 above) and the relationship $\sigma_0 = (e/N_A a)$,[39,40] we can express the last term using the degrees of polymerizations of the blocks only as $(T/a^2)N_B(e/N_A a)^{11/6}\Omega^{11/6}$. To simplify this expression, we will use the notation $C_1 = S - (H/12\pi e^2)$.

The second tem in eq 1, the free energy of the self-similar adsorption structure in the region made of block B, can be expressed using the scaling arguments that have been developed previously:[32,36–38,52]

$$F_B = \Gamma_B\left(\frac{a}{l_0}\right)^{5/3} - \delta a^2\left(\frac{a}{l_0}\right)\Gamma_B \quad (3)$$

The surface coverage $\Gamma_B$ is the number of B monomers per unit area in the hole, $l_0$ is the typical height of the self-similar structure generated from the hole, and $\delta$ is the adsorption parameter that represents the strength of the interaction between monomer B and the surface. The first term is the confinement energy of the adsorbed B blocks and the second is the adsorption energy. As was previously shown,[36–38,52] this term gives a zero energy contribution at equilibrium.

The third term in eq 1 corresponds to the energy needed to form a cylindrical hole in a melt film of the A block and can be written in an analytical form:

$$F_A^{hole} = A\left(\frac{\gamma}{R}\right) \quad (4)$$

The area of the hole is $A = \pi R^2$, where $R$ is the radius of the hole. The term in parentheses gives the Laplace pressure difference between the inside and the outside of the cylindrical hole, where $\gamma$ is the surface tension on the cylinder walls and $(1/R)$ is the mean curvature of the typical cylinder. From the energy per hole we get that the energy needed to form holes in a unit area is given by

$$\Omega F_A^{hole} = \Omega\pi R^2\left(\frac{\gamma}{R}\right) = C_2\Omega^{1/2} \quad (5)$$

This last equality emerges from previous assumptions (stated in item 6 above) that imposes a constant number of holes. Hence, a change of the fractional area of the holes will be equivalent to a change in the area of a single hole and hence, generating the constant $C_2$.

The last term, the interfacial energy term, has the form

$$\Omega F_S = \Omega(2\pi R\gamma e) = 2\pi\gamma e\Omega^{3/2} \quad (6)$$

Substituting eqs 2, 5, and 6 into eq 1 generates the analytical expression for the free energy per unit area of the system:

$$F = (1-\Omega)\left[-C_1 - \gamma_{sA}\left(\frac{e}{N_A a}\right) + \left(\frac{T}{a^2}\right)N_B\left(\frac{e}{N_A a}\right)^{11/6}(1-\Omega)^{5/6}\right] + C_2\gamma\Omega^{1/2} + 2\pi\gamma e\Omega^{3/2} \quad (7)$$

Minimization of the free energy with respect to the partial coverage of the surface $\Omega$ will yield the equilibrium partial coverage of the surface by holes.

$$C_1 + \gamma_{sA}\left(\frac{e}{N_A a}\right) - \left(\frac{11}{6}\right)\left(\frac{T}{a^2}\right)N_B\left(\frac{e}{N_A a}\right)^{11/6}(1-\Omega)^{5/6} + \frac{1}{2}C_2\gamma\Omega^{-1/2} + 3\pi\gamma e\Omega^{1/2} = 0 \quad (8)$$

It is important to note that under the assumption of an independent distribution of the holes (in assumption 5) all the terms of eq 7, with the exception of the first term, are independent of the degree of polymerization of the blocks.

For the case when the spreading power is not large enough to induce the formation of a flat film due to the presence the brush, we can solve eq 8 for two limiting cases:

(a) If we assume that the first term in the square brackets in eq 7 is larger than the second, then we get

**Table 1. Details of a Typical Analysis Using the TGA Measurements for the Determination of the Relative Amounts of PS and PMMA Polymer Moieties Adsorbed Either Directly or Indirectly onto the Surface[a]**

| | PS film | PMMA film | PS−$Al_2O_3$ | PMMA−$Al_2O_3$ |
|---|---|---|---|---|
| fraction | 0.192 | 0.545 | 0.189 | 0.074 |
| mass (mg) | 0.095 | 0.270 | 0.094 | 0.037 |

[a] The experimental and synthetic TGA profiles are shown in Figure 5. The 2.717g sample consisted of a PS47000−PMMA280000 block copolymer adsorbed on 97 nm alumina particles. The total polymer mass was 0.496 mg, which was considered the 100% basis for the calculation of the fraction of each component.

$$(1-\Omega)\approx \text{Const}\cdot\left[\left(\frac{T}{a^2}\right)N_B\left(\frac{e}{N_A a}\right)^{11/6}\right]^{-1}+\Psi(\gamma_{ws},\gamma_{wA},\gamma_{sA}) \quad (9)$$

(b) If we assume that the repulsion between the blocks (second term in eq 7) is the dominant factor in the spreading of the drops, then we obtain

$$(1-\Omega)\approx \text{Const}\cdot\left[\left(\frac{T}{a^2}\right)N_B\left(\frac{e}{N_A a}\right)^{5/6}\right]^{-1}+\Psi(\gamma_{ws},\gamma_{wA},\gamma_{sA}) \quad (10)$$

On the basis of these expressions, we define a new parameter $\epsilon$, the polymeric control parameter, to be $N_B/N_A{}^{11/6}$ in the first limit (eq 9), or $N_B/N_A{}^{5/6}$ in the second limit (eq 10). In both these equations, $\Psi$ is a correction term that depends only on the monomeric interfacial energies and on the particular geometry of the adsorption morphologies.

We should note that eqs 9 and 10 are valid for the case where the correlation length in the top part of the brush is constant. In the case where this correlation length depends also on the degree of polymerization, the second term will include also dependence on the specific polymeric variables. For example, if we take the expression suggested by Binder,[49] we get that the typical radius of the holes scales as

$$R=\Omega^{1/2}N_A{}^{1/6}N_B{}^{2/5} \quad (11)$$

This will translate into a scaling of the variables of the correction term $\Psi$ with the parameter $N_A{}^{1/6}N_B{}^{2/5}$. This scaling parameter has a much weaker dependence on the degrees of polymerization than the scaling parameters in eqs 9 and 10.

## 3. Experimental Methods

**3.1. Materials.** Cyclohexanone, chlorobenzene (spectral grade), 2-ethoxyethanol (spectral grade), and toluene (spectral grade) were purchased from Fisher Scientific and were used without further preparation. Block copolymers (BCP) of PS-*b*-PMMA of varying molecular weights and varying compositions were purchased from Polymer Source Inc.: $PS_{25300}$-*b*-$PMMA_{25900}$, $PS_{47000}$-*b*-$PMMA_{280000}$, $PS_{71300}$-*b*-$PMMA_{11200}$, and $PS_{101100}$-*b*-$PMMA_{165800}$, with PDI ranging from 1.06 to 1.13. Homopolymers of PS and PMMA of various molecular weights were purchased from Alfa Aesar, with PDI values ranging from 1.04 to 1.12. A summary of the various polymers used is given in Table 1. Alumina nanoparticles were purchased from different sources (Nanophase Technologies, Nano-Scale, Reade) depending on the availability of the desired size.

**3.2. Experimental Procedure.** *3.2.1. Preparation of Initial System Mixtures.* 45 mL of 2-methoxyethanol, which is a good solvent for the PMMA block and a bad solvent for the PS block (bp 125 °C, density 0.965 g/cm$^3$), was introduced into a 100 mL Erlenmeyer flask and placed on a Thermolyne Mirak stirring hot plate with the temperature set to 70 °C. A magnetic stirrer was dropped into the flask and began spinning at the preset speed of 200 rpm. 0.603 g of $PS_{101100}$-*b*-$PMMA_{165800}$ was poured into the flask to form a 1.25 vol % diblock copolymer solution. After the polymer was completely dissolved, the stirrer was removed. 0.05 g of alumina ($Al_2O_3$) nanoparticles (Nanophase Technologies, $D_{avg}$ = 37 nm, density 3.97 g/cm$^3$) was measured and kept in weighing paper. The flask was agitated on a Scientific Industries Vortex-2 Genie vortex with a setting of 8−10. While the mixture was swirling continuously the alumina was slowly poured into the flask. Mixing continued for 5 min. The flask was covered with laboratory film and stored in a fume hood for 24 h. Similar experiments were performed with the other diblock copolymer (BCP) molecular weights and compositions, keeping the same polymer volume fraction in all solutions and other sizes of the alumina particles, i.e., $D_{avg}$ = 5 nm, $D_{avg}$ = 97 nm, and $D_{avg}$ = 400 nm.

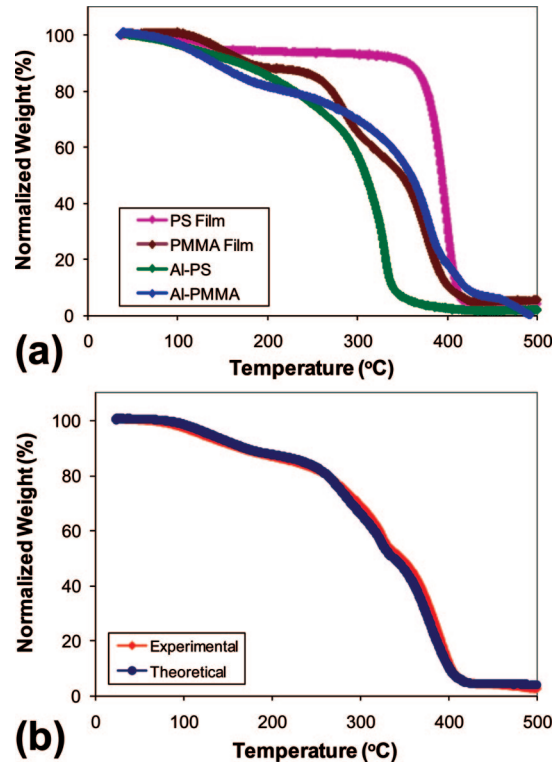


**Figure 5.** An example of the quantitative TGA analysis. (a) The TGA profile of the four individual components. (b) The experimental TGA profile and the corresponding synthetic profile created by the linear combination of all four components. The analysis in this figure is for a sample of 2.717 g consisting of PS47000−PMMA280000 block copolymer adsorbed on 97 nm alumina particles. The total polymer mass was 0.496 mg, which was considered the 100% basis for the calculation of the fraction of each component. Results of the masses of each of the polymer moieties for this sample are summarized in Table 1. Similar calculations were performed with all samples.

Experiments on flat alumina surfaces were performed by first depositing a 1000 Å layer of aluminum onto previously washed Si wafers by electron beam evaporation, using an instrument equipped with a multisample holder mounted on a rotating carriage to ensure even deposition. The thickness of the metal film was measured with a quartz crystal monitor. Immediately upon removal from the evaporator, the freshly prepared aluminum substrates were immersed in a 1.25 vol % 2-methoxyethanol solution of the BCP at 70 °C, similarly to the procedure described previously. The time lapse from the opening of the sample holder of the evaporator and the complete immersion of the samples in the BCP solution was on the average less than 10 min. This allowed the formation of an amorphous native oxide layer on the aluminum surface.[10,55] The BCP solutions with the immersed metal oxide substrates were allowed to mix vigorously for 5 min and then stored at room temperature for 24 h. Excess, unadsorbed polymer was removed by repeated washing with a mixture of toluene and chlorobenzene (Θ-solvents for PMMA and PS, respectively) to generate a stable, chemisorbed BCP film.

*3.2.2. Characterization of Alumina Particle Size.* Transmission electron microscopy (TEM) was used to determine size and distribution of original particles for all polymer suspensions. TEM samples were obtained by placing a small droplet of the reacted solution containing the polymer-coated metal oxide particles onto

a Formvar-coated copper TEM grid from Ted Pella. The grid rested on a thin piece of tissue paper so that the liquid will drain into the paper leaving a very thin film on the grid itself. The TEM analysis was performed on a JEOL 4000 EX high-resolution electron microscope with an operating voltage of 200 keV.

*3.2.3. Characterization of the Adsorbed Diblock Copolymer Layer.* Thermogravimetric analysis (TGA) was conducted to measure the amount of adsorbed polymer. TGA samples were prepared by centrifuging each of the BCP nanocomposite mixtures using Fisher Scientific Centrific Model 228 centrifuge at 10 000−15 000 rpm for 12−17 min. The capped particles formed a solid mass at the bottom of the vial, and excess polymer and solvent solution were removed. The remaining particles were washed with solvent, and the vial was shaken using a Scientific Industries Vortex-2 Genie vortex for 1 min to remove any excess unbound polymer from the particles. The suspension was centrifuged again, and this process was repeated 3−4 times. The particles were placed onto a TGA platinum pan, and the data were collected using a TA Instruments Inc. TGA model 50 at a ramp rate of 10 °C/min to 600 °C.

The thermal degradation mechanism of adsorbed polymers is directly related to the strength of the interaction between the polymer chains and the substrate and, to a lesser degree, the film thickness.[56] Thus, the degradation profile of a polymer mixture (whether in bulk or on a substrate) is given by the appropriately weighted thermal profile of the components.[56–58] The TGA profiles of PS and PMMA differ significantly, either as adsorbed films or as free-standing thin films, thereby enabling the analysis of the composition of the adsorbed films on the surface of the alumina particles. Therefore, the TGA profile expected in our case would consist of a combination of the characteristic thermal decomposition profiles of four different components: adsorbed PMMA on alumina (PMMA−$Al_2O_3$), adsorbed PS on alumina (PS−$Al_2O_3$), free thin PMMA film (equivalent to the unadsorbed PMMA blocks), and free thin PS films (equivalent to unadsorbed PS blocks). These characteristic thermal decomposition profiles were separately obtained from samples containing either PMMA- and PS-coated alumina nanoparticles or free-standing thin films of PMMA and PS. In order to determine the actual composition of our samples, the experimental TGA profile was matched with a synthetic TGA profile constructed from a linear combination of all four components.[25] Figure 5 shows an example of our analysis. Figure 5a shows the TGA profile of the four individual components (as described above), and Figure 5b shows the experimental and synthetic profiles, further used to calculate the various pertinent mass ratios. In this example, the block copolymer consisted of $\bar{M}_{w(PS)} = 47\,000$ g/mol and $\bar{M}_{w(PMMA)} = 280\,000$ g/mol block copolymer adsorbed on alumina nanoparticles with an average diameter of 97 nm. The total sample mass was 2.717 mg. The total polymer mass was 0.496 mg, and the mass of the particles was 2.221 mg. The mass fractions of the four components were calculated on the basis of 0.496 mg of total polymer as 100% and shown in Table 1.

FTIR was used to identify the bonding between the PMMA chains and nanoparticles in the various $Al_2O_3$−BCP systems that we explored. The sample cell was placed inside a Nicolet Instrument Corp. Nexus 870 FT-IR spectrometer sample compartment, and after the latter was sealed and purged for at least 15 min, background spectra were taken and assigned for use on subsequent spectra acquisitions. The vials containing the centrifuged capped particles were shaken using a Scientific Industries Vortex-2 Genie vortex to initiate their resuspension in a hydrocarbon solvent. Using Nicolet OMNIC 5.2a software, the spectra of the capped metal oxide particles were compared against previously recorded spectra of PMMA solutions or PMMA thin films to highlight peaks that are unique to the capped particles.

**3.3. Calculation of Polymer Coverage and Anchoring Density.** The coverage ($\Gamma$) and anchoring density ($\sigma$) of each block on the surface can be calculated by combining the information obtained from TEM, TGA, and FTIR experiments.

*3.3.1. Poly(methyl methacrylate).* The adsorption of the PMMA block onto the $Al_2O_3$ surface (following the hydrolysis of the ester bond and the coordination of the resulting carboxylic group) causes substantial changes in the infrared spectrum in the carbonyl region. The change in the characteristic ratio between the 1687 $cm^{-1}$ absorption band, corresponding to the asymmetric stretch of the $COO^-$ group,[13,60,61] as compared to the 1734 $cm^{-1}$ carbonyl peak for the adsorbed PMMA, $COO^-/C{=}O = E_{1687}/E_{1734}$, provides the relative concentration of the reacted $COO^-$ group.[13,24,60,61] The conformation polymer rearrangement upon adsorption generates a change of the ratio of the 1156 and 1171 $cm^{-1}$ bands, corresponding to the cooperative symmetric and asymmetric stretches of the C—O and C—C bonds of the polymer backbone. The total number of PMMA segments that have anchored to the surface can be calculated from the fraction of the segments containing the bonding group ($COO^-$) that is also experiencing the conformational change, multiplied by the total number of monomers in the sample and divided this by the total number of chains, as follows:[24,32]

$$\frac{N_{anchors}}{N_{chains}} = \frac{E_{1687}}{E_{1734}} \frac{E_{1156}}{E_{1171}} \frac{N_{monomers}}{N_{chains}} \tag{12}$$

Note that the number of chains in the sample (i.e., the number of PMMA chains, which by definition is equal to the total number of BCP chains) can be calculated from the mass fraction of the chemisorbed PMMA block as determined from TGA analysis.

The anchoring density of the PMMA block on the surface of the alumina particles is given by the number of anchoring segments divided by the total surface area of the particles in the sample. TGA data were used to calculate the number of alumina particles in the sample and their resulting surface area as $A_{particles} = N_{particles}\pi\bar{D}_{particles}^2$, where $\bar{D}_{particles}$ is the average diameter of the alumina particles as determined from TEM measurements. The surface density of the PMMA blocks adsorbed on the aluminum oxide particles, $\eta_{PMMA}$, is given by

$$\eta_{PMMA} = \frac{N_{chains}}{A_{particles}} \tag{13}$$

The density of anchoring points of the PMMA blocks per unit area of oxide nanocluster surface (in units of $nm^2$), $\sigma_{PMMA}$, is obtained by the combination of eqs 12 and 13.

*3.3.2. Polystyrene.* The interaction of PS with the alumina surface does not generate significant changes in the FTIR spectrum of the polymer to allow a similar approach as that used for PMMA. Therefore, in this case we have used the experimental TGA and TEM data to calculate both the numbers of anchors per chain (PS block) as well as the coverage. The number of anchors per chain were calculated using the following assumptions: (a) the polymer between two anchoring points behaves as a random coil; (b) the loop formed between two anchoring points is symmetric with only one monomer acting as the pivot point; (c) the density of the adsorbed polymer is similar to that of a very thin PS film; (d) the effective thickness of the PS layer, $L_{eff}$, is considered to be the maximal chain length (Flory's statistical chain length[62]) between the surface and the pivot point and is given by the expression $L_{eff} = [(3/4\pi)(V_{PS} + V_{particles})]^{1/3} - \bar{D}_{particles}/2$. The quantities $V_{PS}$ and $V_{particles}$ are obtained experimentally from the TGA experiments, and the average particle size, $\bar{D}_{particles}$, is obtained from TEM. Hence, the number of anchors per chain is given by the expression

$$\frac{N_{anchors}}{N_{chains}} = \frac{N_{monomers}}{n_{loop}} = \frac{N_{monomers}}{2\left(\frac{L_{eff}}{\sigma l}\right)^2 + 1} \tag{14}$$

The surface density of the PS blocks adsorbed on the aluminum oxide particles, $\eta_{PS}$, is given by

$$\eta_{PS} = \frac{N_{chains}}{A_{particles}} \quad (15)$$

The density of anchoring points of the PS blocks per unit area of oxide nanocluster surface (in units of nm$^2$), $\sigma_{PS}$, is obtained by the combination of eqs 14 and 15.

It is important to mention that, given the nature of the analysis using the TGA profiles of the adsorbed polymers, the extraction of the relative amounts of the four different components on the surface of the particles has a very large associated error margin. Hence, the absolute numbers obtained in this calculation are less important than the qualitative comparison of the numbers obtained for different BCP molecular weights.

## 4. Results and Discussion

The experimental results from the adsorption experiment are shown in Figures 6−8 and are summarized in Table 2. Figure 6 shows the anchoring density (numbers of anchors per nm$^2$) of each block as a function of their respective block molecular weights. Clearly, the anchoring density does not seem to exhibit a particular pattern of dependence on block molecular weight. Conversely, the sum of the anchoring density of both polymers seems to scale linearly with the total molecular weight of the block copolymer, as shown in Figure 7. Finally, Figure 8 shows a similar pattern of behavior for the sum of the individual coverage of both blocks as a function of each block molecular weight (Figure 8a,b) and the total molecular weight of the block copolymers. The results summarized in Table 2 are calculated on the basis of the data in these figures. The first row in each entry gives the coverage $\Gamma_A$ by the monomers of the PS, and the second row gives $\Gamma_B$, the coverage by the PMMA monomers. In both cases the coverage is normalized to the total sphere surface area. Data analysis of the experimental results can be used to find the composition of the modeled adsorption structure.

**Table 2. Summary of the Coverage $\Gamma_A$ and $\Gamma_B$ of the A and B Monomers (per nm$^2$) in the Adsorption Layer[a]**

| $N_AN_B$ | | 686112 | 243259 | 4521658 | 9722800 |
|---|---|---|---|---|---|
| $D_{avg}$ = 5 nm | $\Gamma_A$ | 1.26 | 0.28 | 1.01 | 0.68 |
| | $\Gamma_B$ | 0.17 | 0.28 | 1.73 | 2.61 |
| $D_{avg}$ = 37 nm | $\Gamma_A$ | 10.28 | 7.20 | 7.00 | 10.17 |
| | $\Gamma_B$ | 3.36 | 4.31 | 2.60 | 2.52 |
| $D_{avg}$ = 97 nm | $\Gamma_A$ | 26.87 | 16.69 | 18.36 | 16.87 |
| | $\Gamma_B$ | 7.79 | 8.21 | 6.81 | 6.60 |
| $D_{avg}$ = 400 nm | $\Gamma_A$ | 124.49 | 72.02 | 105.10 | 117.97 |
| | $\Gamma_B$ | 26.89 | 43.09 | 31.82 | 27.22 |

[a] The measurements were performed using a variety of adsorbing particle sizes and different blocks molecular weights.

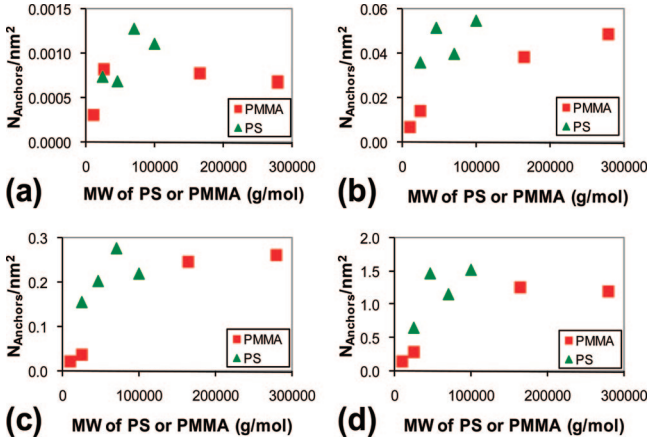


**Figure 6.** Anchoring density (numbers of anchors per nm$^2$) of each block, PS ($\sigma_A$, green) and PMMA ($\sigma_B$, red), as a function of their respective block molecular weights: (a) 5 nm particles; (b) 37 nm particles; (c) 97 nm particles; (d) 400 nm particles.

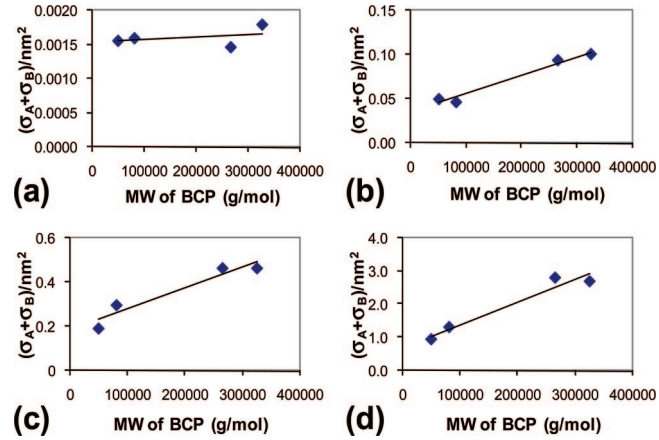


**Figure 7.** Sum of the anchoring density of both polymers, $\sigma_A + \sigma_B$, as a function of the total molecular weight of the block copolymer: (a) 5 nm particles; (b) 37 nm particles; (c) 97 nm particles; (d) 400 nm particles.

The measured surface coverage was averaged over the surface area of the sphere. Thus, the real coverage will be

$$\Gamma_A = \left(\frac{4\pi R^2}{4\pi R^2 - S_B}\right)\Gamma_A' \quad \text{and} \quad \Gamma_B = \left(\frac{4\pi R^2}{S_B}\right)\Gamma_B' \quad (16)$$

where $\Gamma_A'$ and $\Gamma_B'$ are the experimental coverages of blocks A and B from Table 2 and $S_B$ is the area covered by polymer B. In our previous work, we found that under similar solvent conditions, i.e., good solvent for PMMA,[32] the coverage of adsorbed PMMA homopolymers on the same type of surfaces is independent of molecular weight but dependent only on surface curvature, yielding the following results (in units monomers/nm$^2$): $\Gamma_{PMMA}(400) = 66$, $\Gamma_{PMMA}(97) = 19$, and $\Gamma_{PMMA}(39) = 6.7$.

In order to calculate the relative coverage of the self-similar structure of the PMMA block in the current case ($\Omega$), we compared the above results[32] to those in Table 2. The ratio of the two quantities can be used to generate the approximate relation:

$$\Gamma_B \approx 0.4(\Gamma_A + \Gamma_B) \quad (17)$$

For the case of dilute to semidilute polymer solutions, the coverage is independent of the concentration. This fact, coupled with the relation between the real coverage and the measured coverage (eq 16), leads to the expression $S_B = 4\pi R^2/2.5$, i.e., the area covered by the self-similar adsorption structure formed by the PMMA blocks cover about 0.4 of the surface of the spheres. From this observation, we can try to approximate the validity of the two models that we have introduced in the previous section.

First, we will try to estimate the geometry of the melt on the surface. If we assume that the melt has the shape of a drop (for the drop model), then the height and width of the drops can be determined from the experimental results. The relative amount of surface covered by the melt of block A will be 0.6 of the surface area. Using this, one finds that the actual surface coverage with the PS monomers $\bar{D}_{particle} = 400$ nm is approximately $\Gamma_A = 110$. The partial coverage per adsorption site, $\Gamma_A a^2 \approx 5$, is the number of PS monomers per surface adsorption site or, for the melt conditions, the average height of the drop. To approximate the radius of the drop, we will employ the expression for the aggregation number of polymers in a surface micelle: $q^{surface} = f(\theta)N_B^{-3/11}N_A^{10/11}$. In this expression, $q^{surface}$ is the surface aggregation number and $f(\theta)$ is a geometrical factor that depends on the contact angle of the drop.[51] If the drop has a noticeable curvature, then this function will be

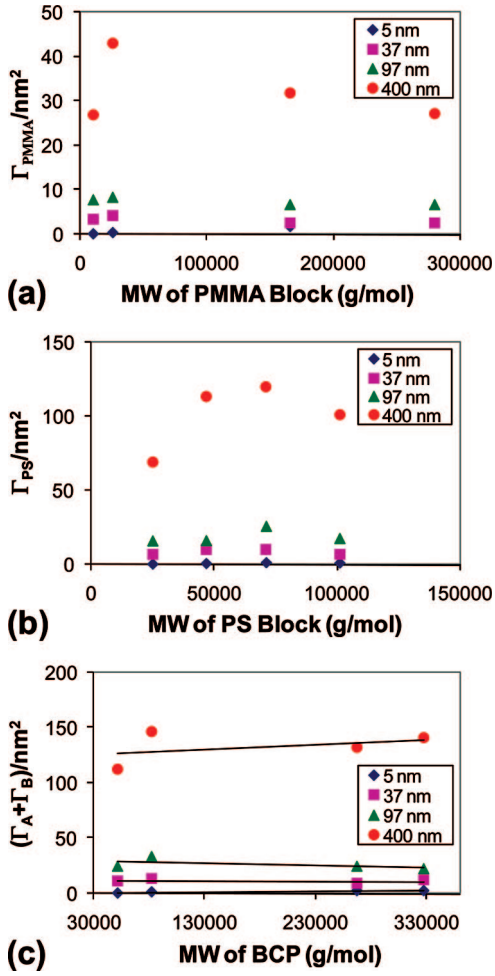


**Figure 8.** Sum of the individual coverages of both blocks ($\Gamma_A$ for PS and $\Gamma_B$ for PMMA): (a) $\Gamma_A + \Gamma_B$ as a function of the molecular weight of the PS block; (b) $\Gamma_A + \Gamma_B$ as a function of the molecular weight of the PMMA block; (c) $\Gamma_A + \Gamma_B$ as a function of the total molecular weight of the block copolymers.

approximately equal to one. From this equation, we can estimate an aggregation number of 100 in our drops. If we assume that in the typical case $N_A = 1000$, we get that there are about 100 000 monomers in the drop. From the number of monomers and from the average height of the drops, we get that the radius of the drop has an approximate value of 100 monomers. Hence, the height of the given drop is much smaller than its radius, which indicates that the drops are very flat ("pancake" shape). The drop model is valid only when the contact angle is much larger than zero, and hence, this is obviously not supported by our experimental results.

A second assumption of the drops model is that the drops do not interact with each other. Since we are assuming that each drop has a corona with a brush-like structure, this assumption is equivalent to the condition that the distance between the boundaries of two drops will be larger than twice that of the brush height. This height is calculated from the expression $L \approx N_B/N_A^{1/3}n_e$,[39,40] where $n_e$ is the average height of the melt in monomeric units. If we assume that $N_B = N_A = 1000$, we get that the brush height is equivalent to several hundred monomers. From the fractional area covered by the drops and from the approximation of the drop radius ($R = 100$ monomers), we get that the average distance between the drops is of the order of 20 monomers, which is much less than the critical interaction length. This fact leads to a second violation of the assumptions on which the drop model is based.

**Table 3. Summary of the Partial Surface Area, Ω, Covered by the B (PMMA) Blocks Having the Self-Similar Structure That Is Characteristic of an Adsorbed Polymer Layer from a Good Solvent with Favorable Surface Interactions**

| $N_AN_B$ | 686112 | 243259 | 4521658 | 9722800 |
|---|---|---|---|---|
| $D_{avg} = 37$ nm | 0.50 | 0.60 | 0.40 | 0.35 |
| $D_{avg} = 97$ nm | 0.40 | 0.45 | 0.35 | 0.35 |
| $D_{avg} = 400$ nm | 0.40 | 0.65 | 0.45 | 0.40 |

The experimental results in this work that indicate that the adsorption region is composed of a homogeneous thin film of melt, and this is consistent with the perforated film model rather than the drops model.[63] The coverage ratio between $N_A$ and $N_B$ shows that the majority of the surface is covered by the solvophobic block (melt), while the minority coverage is by a solution of the solvophilic block. This fact strengthens our assumption that adsorption of the B blocks forms circular holes in the melt film of block A. When testing the validity of the theory with the experimental results, we have to keep in mind that a multistage calculation was needed to extract the experimental coverage, and hence we anticipate a large error in these parameters. Because of this limitation, any comparison will be qualitative only.

The correspondence of the experimental results with the theoretical predictions of eqs 9 and 10 can be tested by checking the partial coverage of the B block as a function of $\epsilon$, the polymeric control parameter, and is shown in Table 3. The experimental results indicate only small variations in the partial coverage of the alumina, even though the theory predicts a greater dependence on the molecular weights of the block through the polymer control parameter $\epsilon$. A possible explanation for these variations can be traced to the enforced geometry of the adsorbed layer. Any other choice for the structure of the adsorbed layer, i.e., a different hole size and distribution as a function of $N_A$ and $N_B$ of the adsorption layer, will most likely translate into modifications to the $\Psi$ term in eqs 9 and 10.

## 5. Conclusions

The results of our experiments indicate that block copolymers with different chemical reactivities in a selective solvent undergo a competitive adsorption onto alumina surfaces. When the solvent is bad for the PS block and good for the PMMA block, both blocks compete for adsorption on the alumina surface for two completely different reasons. The PS is attracted to the surface due its incompatibility with the solvent, while the PMMA is attracted to surface due to the relatively strong interactions of its segments with the surface. Hence, the structure of the adsorbed layer is a result of the parallel occurrence of the two different phenomena.

Two theoretical models, the modified drops model and the perforated film model, have been evaluated as appropriate representation of such an adsorption scenario. Evidently, the experimental results indicate that the model that is valid for our case is that of a perforated film structure. Such a perforated film can have different hole geometries, even though in this study we have explored only the circular hole option with a constant distribuand tion. The adsorption of the PS−PMMA block copolymer generates a patterned surface comprised of a homogeneous melt layer of the PS block perforated with holes having a variable PMMA structure, depending on the distance from the bottom of the hole (alumina surface). The density gradient of the PMMA moiety in the hole reverts to a classical brush morphology at a critical distance from the surface of the hole. The partial coverage of the surface can be scaled with the polymer control parameter $\epsilon$, which is a ratio of the molecular weights of the two blocks. Variations in the control parameter coupled with variations in the geometry of the holes in the perforated layer can result in major differences in the adsorbed

layer morphology. This fact indicates that with proper control of adsorption parameters it would be possible to pattern of the surface according to specific design requirements.

**Acknowledgment.** This work was supported in part by grants from NSF, AFOSR, ARO, MURI, and MRI-HEL as well as by a grant from NIH (NAC P41 RR-13218) through Brigham and Women's Hospital. This work is part of the National Alliance for Medical Image Computing (NAMIC), funded by the National Institutes of Health through the NIH Roadmap for Medical Research, Grant U54 EB005149. Information on the National Centers for Biomedical Computing can be obtained from http://nihroadmap.nih.gov/bioinformatics. Allen Tannenbaum is also with the Department of Electrical Engineering, Technion, Israel, where he is supported by a Marie Curie Grant through the European Union (EU). This research was also supported by the National Science Foundation, Grant No. 0704006, and by the National Institutes of Health, through the Centers of Cancer Nanotechnology Excellence: Emory−GT Nanotechnology Center for Personalized and Predictive Oncology, Award No. 5-40255-G1: CORE 1. Rina Tannenbaum is also with the department of Chemical Engineering, Technion, Israel, where she is supported by a Marie Curie Grant through the European Union (EU) and by the Israel Science Foundation, Grant No. 650/06.

## References and Notes

(1) Cohen Stuart, M. A.; Van Eijk, M. C. P.; Dijt, J. C.; Hoogeveen, N. G. *Macromol. Symp.* **1997**, *113*, 163–175.
(2) Li, S.-B.; Zhang, L.-X. *J. Polym. Sci., Polym. Phys.* **2006**, *44*, 2888–2901.
(3) Van der Beek, G. P.; Cohen Stuart, M. A. *J. Phys. (Paris)* **1988**, *49*, 1449–54.
(4) Li, Y.; Huang, Q.; Shi, T.; An, L. *J. Phys. Chem. B* **2006**, *110*, 23502–23506.
(5) Nakaya, K.; Imai, M.; Komura, S.; Kawakatsu, T.; Urakami, N. *Europhys. Lett.* **2005**, *71*, 494–500.
(6) Andelman, D.; Joanny, J. F. *Macromolecules* **1991**, *24*, 6040–6042.
(7) Netz, R. R.; Andelman, D. *Surfactant Sci. Ser.* **2001**, *103*, 115–155, and pertinent references therein.
(8) Bjelopavlic, M.; El-Shall, H.; Moudgil, B. M. *Surfactant Sci. Ser.* **2002**, *104*, 105–133.
(9) Crispin, X.; Lazzaroni, R.; Geskin, V.; Baute, N.; Dubois, P.; Jerome, R.; Bredas, J. L. *J. Am. Chem. Soc.* **1999**, *121*, 176–187.
(10) Peyser, P.; Tutas, D. J.; Stromberg, R. R. *J. Polym. Sci., Polym. Chem.* **1967**, *5*, 651–63.
(11) Dan, N. *Langmuir* **2000**, *16*, 4045–4048.
(12) Tsivline, D.; Stepanyuk, V. S.; Levanov, N.; Hergert, W.; Katsnelson, A. A. *Comput. Phys. Commun.* **1999**, *121*, 747.
(13) Kostandinidis, F.; Thakkar, B.; Chakraborty, A. K.; Potts, L.; Tannenbaum, R.; Tirrell, M.; Evans, J. *Langmuir* **1992**, *8*, 1307.
(14) Di Marzio, E. A. *J. Polym. Sci., Polym. Phys.* **2006**, *44*, 2612–2620.
(15) Shang, L.; Qin, C.; Wang, T.; Wang, M.; Wang, L.; Dong, S. *J. Phys. Chem. C* **2007**, *111*, 13414–13417.
(16) Favier, I.; Gomez, M.; Muller, G.; Picurelli, D.; Nowicki, A.; Roucoux, A.; Bou, J. *J. Appl. Polym. Sci.* **2007**, *105*, 2772–2782.
(17) Starkey Ott, L.; Hornstein, B. J.; Finke, R. G. *Langmuir* **2006**, *22*, 9357–9367.
(18) Dan, N.; Zubris, M.; Tannenbaum, R. *Macromolecules* **2005**, *38*, 9243–9250.
(19) Skirtach, A. G.; Dejugnat, C.; Braun, D.; Susha, A. S.; Rogach, A. L.; Sukhorukov, G. B. *J. Phys. Chem. C* **2007**, *111*, 555–564.
(20) Kang, Y.; Taton, T. A. *Macromolecules* **2005**, *38*, 6115–6121.
(21) Tannenbaum, R.; King, S.; Hyunh, K.; Zubris, M.; Dan, N. *Mater. Res. Soc. Symp. Proc.* **2003**, *788*, 3–11.
(22) Surve, M.; Pryamitsyn, V.; Ganesan, V. *Langmuir* **2006**, *22*, 969–981.
(23) Tannenbaum, R.; Zubris, M.; Goldberg, E. P.; Reich, S.; Dan, N. *Macromolecules* **2005**, *38*, 4254–4259.
(24) Ciprari, D.; Jacob, K.; Tannenbaum, R. *Macromolecules* **2006**, *39*, 6565–6573.
(25) David, K.; Dan, N.; Tannenbaum, R. *Surf. Sci.* **2007**, *601*, 1781–1788.
(26) Park, M.-K.; Youk, J. H.; Pispas, S.; Hadjichristidis, N.; Advincula, R. *Langmuir* **2002**, *18*, 8040–8044.
(27) Chandekar, A.; Sengupta, S. K.; Barry, C. M. F.; Mead, J. L.; Whitten, J. E. *Langmuir* **2006**, *22*, 8071–8077.
(28) Oslanec, R.; Costa, A. C.; Composto, R. J.; Vlcek, P. *Macromolecules* **2000**, *33*, 5505–5512.
(29) Nowicki, W. *Macromolecules* **2002**, *35*, 1424.
(30) Skau, K. I.; Blokhuis, E. M. *Macromolecules* **2003**, *36*, 4637–4645.
(31) Gorbunov, A. A.; Zhulina, E. B.; Skvortsov, A. M. *Polymer* **1982**, *23*, 1133–1142.
(32) Hershkovitz, E.; Tannenbaum, A.; Tannenbaum, R. *J. Phys. Chem. C* **2007**, *111*, 12369–12375.
(33) Ding, Y.; Sokolov, A. P. *J. Polym. Sci., Polym. Phys.* **2004**, *42*, 3505–3511.
(34) Siline, M.; Leonov, A. I. *Polymer* **2002**, *43*, 5521–5525.
(35) Aubouy, M.; Dimeglio, J. M.; Raphael, E. *Europhys. Lett.* **1993**, *24*, 87.
(36) De Gennes, P. G. *Macromolecules* **1981**, *14*, 1637–44.
(37) De Gennes, P. G. *Adv. Colloid Interface Sci.* **1987**, *27*, 189–209.
(38) De Gennes, P. G. *J. Phys. (Paris)* **1976**, *37*, 1445–52.
(39) Marques, C.; Joanny, J. F. *Macromolecules* **1988**, *21*, 1051–59.
(40) Marques, C.; Joanny, J. F. *Macromolecules* **1989**, *22*, 1454–58.
(41) Washington, C.; King, S. M.; Attwood, D.; Booth, C.; Mai, S.-M.; Yang, Y.-W.; Cosgrove, T. *Macromolecules* **2000**, *33*, 1289–1297.
(42) Striolo, A.; Jayaraman, A.; Genzer, J.; Hall, C. K. *J. Chem. Phys.* **2005**, *123*, 064710/1–064710/15.
(43) Siqueira, D. F.; Breiner, U.; Stadler, R.; Stamm, M. *Langmuir* **1995**, *11*, 1680–1687.
(44) Tassin, J. F.; Siemens, L. R.; Tang, T. W.; Hadziioannou, G.; Swalen, D. J.; Smiths, A. B. *J. Phys. Chem.* **1989**, *93*, 2106–2111.
(45) O'Shea, S. J.; Welland, M. E.; Rayment, T. *Langmuir* **1993**, *9*, 1826–1835.
(46) Kramarenko, E. Y.; Potemkin, I. I.; Khokhlov, A. R.; Winkler, R. G.; Reinker, P. *Macromolecules* **1999**, *32*, 3495–3501.
(47) Meiners, J. C.; Quintel-Ritzi, A.; Mlynek, J.; Elbs, H.; Krausch, G. *Macromolecules* **1997**, *30*, 4945–4951.
(48) Spatz, J. P.; Sheiko, S.; Moller, M. *Macromolecules* **1996**, *29*, 3220–3226.
(49) Binder, K. *Eur. Phys. J. E* **2002**, *9*, 293–298.
(50) Zhan, Y.; Mattice, W. L. *Macromolecules* **1994**, *27*, 683–688.
(51) Ligoure, C. *Macromolecules* **1991**, *24*, 2968–2972.
(52) De Gennes, P. G. *Scaling Concepts in Polymers Physics*; Cornell University Press: Ithaca, NY, 1979.
(53) Alexander, S. *J. Phys. (Les Ulis, Fr.)* **1977**, *38*, 983.
(54) Seemann, R.; Herminghaus, S.; Neto, C.; Schlagoski, S.; Podzimek, D.; Konrad, R.; Mantz, H.; Jacobs, K. B. *J. Phys.: Condens. Matter* **2005**, *17*, S267–S290.
(55) Skirtach, A. G.; Dejugnat, C.; Braun, D.; Susha, A. S.; Rogach, A. L.; Sukhorukov, G. B. *J. Phys. Chem. C* **2007**, *111*, 555–564.
(56) Aymonier, C.; Bortzmeyer, D.; Thomann, R.; Müllhaupt, R. *Chem. Mater.* **2003**, *15*, 4874.
(57) Kuljanin, J.; Marinovic-Cincovic, M.; Zec, S.; Comor, M. I.; Nedeljkovic, J. M. *J. Mater. Sci. Lett.* **2003**, *22*, 235.
(58) Zhang, B.; Blum, F. D. *Thermochim. Acta* **2003**, *396*, 211.
(59) Chuai, C.; Almdal, K.; Lyngaae-Jørgensen, J. *J. Appl. Polym. Sci.* **2004**, *91*, 609.
(60) Tannenbaum, R.; Hakanson, C.; Zeno, A. D.; Tirrell, M. *Langmuir* **2002**, *18*, 5592.
(61) Tannenbaum, R.; King, S.; Lecy, J.; Tirrell, M.; Potts, L. *Langmuir* **2004**, *20*, 4507.
(62) Gmachowski, L. *Polymer* **2007**, *48*, 4316–4321.
(63) Hajduk, D. A.; Takenouchi, H.; Hillmyer, M. A.; Bates, F. S.; Vigild, M. E.; Almdal, K. *Macromolecules* **1997**, *30*, 3788–3795.

MA702706P